

A Computational Study of Acid Catalyzed Aerosol Reactions of Atmospherically Relevant Epoxides

Ivan R. Piletic¹, Edward O. Edney¹, Libero J. Bartolotti²

¹United States Environmental Protection Agency, National Exposure Research Laboratory, Research Triangle Park, NC 27711.

²East Carolina University, Department of Chemistry, Greenville, NC 27858.

Abstract

Epoxides are important intermediates of atmospheric isoprene oxidation. Their subsequent reactions in the particle phase lead to the production of organic compounds detected in ambient aerosols. We apply density functional theory to determine the important kinetic factors that drive epoxide reactions in the particle phase. Specifically, the importance of acid catalysis and solvent polarity are investigated using a variety of epoxides and nucleophiles. The condensed phase is modeled using molecular clusters immersed in a dielectric continuum and a majority of the calculations are performed with the M062x density functional and 6-311++G** basis set. Calculations of acid catalyzed epoxide hydrolysis transition states for simple primary, secondary and tertiary epoxides are consistent with an A-2 mechanism where the nucleophile (water) interacts with an epoxide carbon in the transition state. By applying transition state theory to this mechanism, the overall rate constants of epoxide reactions such as hydrolysis, organosulfate formation, organonitrate formation and oligomerization are determined. The calculations indicate that the acid catalyzed hydrolysis rate constant of 2-methyl-2,3-epoxybutane-1,4-diol (β -IEPOX - an isoprene epoxide produced under low NO_x conditions) is approximately 30 times greater than 2-methyl-2,3-epoxypropanoic acid (MAE - methacrylic acid epoxide derived from isoprene and produced at high NO_x concentrations). Furthermore, acid catalyzed organosulfate formation and epoxide oligomerization reactions are competitive and appear kinetically favorable over the hydrolysis of IEPOX.

Introduction

Fine particulate matter (PM_{2.5} – particles smaller than 2.5 μm) is a regulated criteria air pollutant that presents a significant health burden and affects the earth's climate.¹⁻³ Numerous biogenic and anthropogenic sources contribute to aerosol particle growth with organic constituents representing a significant mass fraction.⁴ The organic aerosols may be directly emitted (primary organic aerosol or POA) or they may be generated from volatile species that oxidize in the atmosphere and condense onto growing aerosol particles (secondary organic aerosol or SOA). SOA represents a substantial mass fraction of submicrometer atmospheric aerosol⁵ and is particularly pronounced during the warmer seasons which are conducive to photochemistry and biogenic emissions.

Isoprene (2-methyl-1,3-butadiene) is the largest unsaturated biogenic hydrocarbon source emitted into the atmosphere. Its reactions with powerful atmospheric oxidants such as the hydroxyl radical or ozone give rise to semi-volatile intermediates that are more likely to condense onto growing aerosol particles where they may react further.⁶ Other reactants such as NO_x and sulfate may also participate in the oxidation pathway giving rise to low volatility products thereby linking biogenic and anthropogenic aerosol chemistry in the atmosphere.⁷ Specific isoprene derived compounds have been detected in laboratory chambers and ambient aerosols such as 2-methyl tetrol,⁸ methyl glyceric acid⁹ and organosulfates.¹⁰ While product distributions of such compounds provide constraints in atmospheric model outputs, they do not afford essential kinetic parameters that are necessary to model time dependent atmospheric isoprene chemistry. It is therefore not only imperative to identify reaction intermediates and products but also to assess the relative reactivities of the pathways linking the two. Only under such circumstances, may the atmospheric chemistry of isoprene be effectively modeled.

Recent studies have identified epoxides as intermediates in the atmospheric oxidation of isoprene. Paulot *et al.* identified epoxydiols (isoprene epoxide - IEPOX) as major reactive intermediates

of isoprene oxidation under low-NO_x conditions.¹¹ Recently, Lin *et al.* have shown that an epoxy-carboxylic acid (methacrylic acid epoxide - MAE) is a significant precursor of SOA formation from isoprene photooxidation under high-NO_x conditions.¹² Epoxides are known to be taken up by acidic solutions¹³ and aerosols¹⁴ where they may participate further in ring opening reactions. Recent kinetic studies involving alkyl, alkenyl and more oxidized epoxides^{15, 16} illustrate that such ring opening reactions are favorable under ideal pH and hydration conditions. Eddingsaas *et al.* estimated a hydrolysis rate constant for IEPOX in acidified aqueous solutions using kinetic measurements on a number of similarly structured epoxides.¹⁶ To date, no estimation or measurement of the MAE hydrolysis rate constant has been made. While these studies have been crucial in quantifying the reaction kinetics of atmospheric epoxides, the kinetic measurements are typically carried out in neat solutions that are not representative of the chemical complexity contained in aerosols. Different acids, varying levels of hydration and a variety of reactive compounds all affect the aerosol phase chemistry of atmospheric epoxides. In this work, we apply density functional theory and transition state theory to calculate epoxide reaction rate constants in the condensed phase under a variety of reaction conditions that may be applicable to aerosol chemistry. In particular, the influence of factors such as solvent polarity and the identity of acid or nucleophile are systematically examined in a variety of ring opening reactions involving these epoxides.

Theory

Rate constants are calculated using the expression from conventional transition state theory which treats the reacting system as a quasi-equilibrium between reactants and an activated complex,¹⁷

$$k = \frac{k_B T}{h C_0^{n-1}} \exp\left(-\frac{\Delta G_{act}^0(T)}{RT}\right) \quad (1)$$

where k_B is Boltzmann's constant, T is the temperature, h is Planck's constant, C_0 is the concentration corresponding to the standard state, n is the molecularity of the reaction ($n = 1$ for unimolecular and 2 for bimolecular) and $\Delta G_{act}^o(T)$ is the standard molar free energy of activation. Equation 1 does not consider barrier recrossings¹⁸ or quantum tunneling effects¹⁹ which are not considered here. Details of the computational model and approximations used to calculate $\Delta G_{act}^o(T)$ of epoxide reactions in the liquid phase are provided in the Supporting Information and are only briefly outlined here.

Equation 1 illustrates that $\Delta G_{act}^o(T)$ is fundamental to computing a rate constant and requires that the free energy surface (FES) of a solute/solvent system is properly defined. The solvation of a solute may be approximated using either explicit (discrete) or implicit (continuum) solvation models.²⁰ Hybrid models that incorporate some explicit solvent molecules around a solute (thereby forming a supersolute) immersed in a solvent bath continuum are appealing because they may avoid the disadvantages of either purely explicit or implicit models.²¹ In this work, a hybrid model was used to describe a variety of epoxide ring opening reactions in the condensed phase which is described in detail in the computational methods section.

When a continuum model is used, the FES or statistical mechanical potential of mean force,²² $W(\mathbf{R})$ for an N atom solute (or supersolute) with fixed $3N-6$ nuclear coordinates at \mathbf{R} is given by,

$$W(\mathbf{R}) = V(\mathbf{R}) + \Delta G_S^*(\mathbf{R}) \quad (2)$$

where $V(\mathbf{R})$ denotes the gas phase potential energy surface and $\Delta G_S^*(\mathbf{R})$ is the free energy of solvation with nuclei clamped and fixed standard state concentrations. The choice of a particular standard state is made by computational convenience or by following convention (standard state solute concentrations of 1 mol/L are used in this work). While $\Delta G_S^*(\mathbf{R})$ depends on the choice of standard state, the rate constant does not because the standard state concentrations also appear in the denominator of the pre-

exponential term in Equation 1 which has a cancelling effect as will be shown in the discussion that follows.

It is important to understand that the FES from Equation 2 pertains to solutes with fixed nuclei at R . According to Ben-Naim,^{23, 24} an additional entropy term to the molar Gibbs free energy (chemical potential) is required to allow the species to move around in the solution volume. The molar Gibbs free energy of a species i in solution may be expressed as,

$$G_i = G_i^* - TS_{lib,i} \quad (3)$$

The first term G_i^* is the chemical potential of a species with fixed nuclei in solution (pseudochemical potential). The second term has been called the liberation free energy²³ and contains the absolute temperature T and the entropy of liberation $S_{lib,i}$ for species i ,

$$S_{lib,i} = -R \ln(C_i N_A \Lambda_i^3) \quad (4)$$

where R is the gas constant, C_i is the concentration of i in moles per unit volume, N_A is Avogadro's number and Λ_i is the thermal de Broglie wavelength defined by,

$$\Lambda_i = h(2\pi m_i k_B T)^{-1/2} \quad (5)$$

in which m_i is the mass of species i . The $\Delta G_{act}^o(T)$ may now be computed using Equations 3 – 5 and the following,

$$\Delta G_{act}^o(T) = \Delta G_{act}^*(T) - T\Delta S_{lib,act}(T) \quad (6)$$

where $\Delta G_{act}^*(T)$ is the difference in internal free energy between the transition state and reactant complexes (pseudochemical potential energy difference). In the calculations presented, $\Delta G_{act}^*(T)$ is approximated using the zero point inclusive electronic energies with vibrational frequencies calculated in solution using a continuum model.²⁵ $\Delta S_{lib,act}$ is the difference in liberation entropy between the

transition state and separate reactant species. It contains the standard state concentrations (see Equation 4) which cancel the concentration term in the denominator of Equation 1 so that the rate constant does not depend on the choice of standard state. Equations 1 and 6 provide a means to estimate liquid phase rate constants for atmospherically relevant epoxide reactions.

Kinetic Model

The previous section detailed the theoretical framework that is used to calculate liquid phase rate constants for single step reactions. In many instances however, reaction pathways involve multiple steps that need to be accounted for to determine an overall rate constant.²⁶ In acid catalyzed epoxide hydrolysis reactions, several elementary steps occur during the conversion of reactants to products. Additionally, two distinct reaction pathways known as A-1 and A-2 are possible.²⁷ The A-1 mechanism (analogous to the S_N1 substitution mechanism) involves four steps whereby an acid (such as H_3O^+) protonates the epoxide oxygen, the epoxide ring opens forming a carbocation followed by nucleophilic attack of water with a subsequent deprotonation forming the final diol moiety. Figure 1a displays a schematic diagram of the FES for this reaction. The rate determining step for this mechanism is the formation of the carbocation which is stabilized in highly substituted epoxides (containing aliphatic groups). The A-2 mechanism (analogous to S_N2) is a three step mechanism whereby an acid protonates the epoxide oxygen, the epoxide ring opens as the nucleophile attacks with subsequent deprotonation once again yielding the diol functional group. Figure 1b shows the FES for the A-2 mechanism. In this case, steps two and three of the A-1 mechanism are effectively combined with the rate determined by the concerted ring opening and nucleophilic attack of the epoxide ring. Less substituted epoxides reacting in solvents of reduced polarity favor this mechanism.

Given the rate determining step, rate law expressions and overall rate constants may be derived for each mechanism. In the A-1 mechanism, the rate law may be expressed as,

$$-\frac{d[\text{epoxide}]}{dt} = k_2[\text{epoxide} - H^+] \quad (7)$$

where k_2 is a first order rate constant (s^{-1}). Assuming a pre-equilibrium exists between the epoxide and the protonated epoxide, $[\text{epoxide} - H^+]$ may be related to the reactants via the equilibrium constant expression,

$$K_1 = \frac{a_{\text{epoxide}-H^+}}{a_{\text{epoxide}} \cdot a_{H^+}} = \frac{\frac{\gamma_{\text{epoxide}-H^+}[\text{epoxide}-H^+]}{C_{0,\text{epoxide}-H^+}}}{\frac{\gamma_{\text{epoxide}}[\text{epoxide}]}{C_{0,\text{epoxide}}} \frac{\gamma_{H^+}[H^+]}{C_{0,H^+}}} = \frac{1M \cdot [\text{epoxide}-H^+]}{[\text{epoxide}] \cdot [H^+]} \quad (8)$$

where the equilibrium constant K_1 is dimensionless and calculated using chemical activities. In deriving the final expression in Equation 8, all activity coefficients γ are assumed to be 1 and all standard state concentrations $C_{0,i}$ are 1 M. Equation 8 may be substituted in Equation 7 to derive the following rate law expressed as a function of the initial reactants,

$$-\frac{d[\text{epoxide}]}{dt} = \frac{K_1 k_2}{1M} [\text{epoxide}][H^+] \quad (9)$$

The overall rate constant for the A-1 mechanism is therefore,

$$k_{A-1} = \frac{K_1 k_2}{1M} \quad (10)$$

which has units of $M^{-1}s^{-1}$ and the reaction that has an overall order of 2. Equation 1 and the relationship between an equilibrium constant and the ΔG of a reaction may be used to express k_{A-1} in terms of the FES of the reaction,

$$k_{A-1} = \frac{\exp\left(-\frac{\Delta G_1}{RT}\right) \left(\frac{k_B T}{h} \exp\left(-\frac{\Delta G_2^\ddagger}{RT}\right) \right)}{1M} = \frac{k_B T}{h(1M)} \exp\left(-\frac{\Delta G_1 + \Delta G_2^\ddagger}{RT}\right) \quad (11)$$

It is evident from Equation 11 that the free energy of the protonated epoxide intermediate is unnecessary to calculate in a cluster calculation involving an acid, water and epoxide provided that a

pre-equilibrium exists between the acid and the protonated epoxide. Only the reactant cluster and the ring opened transition state need to be calculated thereby giving rise to the sum $\Delta G_1 + \Delta G_2^\ddagger$.

A similar kinetic analysis may be carried out for the A-2 mechanism. The fundamental difference between this mechanism and the A-1 mechanism is that the rate determining step also depends on the concentration of the nucleophile (water). The A-2 rate law may be expressed as,

$$-\frac{d[\text{epoxide}]}{dt} = k_2[\text{epoxide} - H^+][H_2O] \quad (12)$$

where k_2 is now a second order rate constant ($M^{-1}s^{-1}$). Once again, assuming a pre-equilibrium exists between the epoxide and the protonated epoxide, Equation 8 may be used to derive the overall rate law,

$$-\frac{d[\text{epoxide}]}{dt} = \frac{K_1 k_2}{1M} [\text{epoxide}][H^+][H_2O] \quad (13)$$

The overall rate constant for the A-2 mechanism is therefore,

$$k_{A-2} = \frac{K_1 k_2}{1M} \quad (14)$$

which has units of $M^{-2}s^{-1}$ and the reaction that has an overall order of 3. In terms of the FES, k_{A-2} is expressed as,

$$k_{A-2} = \frac{\exp\left(-\frac{\Delta G_1}{RT}\right) \left(\frac{k_B T}{h(1M)} \exp\left(-\frac{\Delta G_2^\ddagger}{RT}\right) \right)}{1M} = \frac{k_B T}{h(1M)^2} \exp\left(-\frac{\Delta G_1 + \Delta G_2^\ddagger}{RT}\right) \quad (15)$$

Equations 11 and 15 appear to be the same except for the standard concentration term in the denominator which affects the units of the rate constant. The other more significant difference is that the free energies of activation for a specific epoxide are different depending on which pathway (A-1

versus A-2) is taken. Ultimately, the pathway with the lowest barrier will determine what mechanism is the dominant one for a particular epoxide.

Equations 9 and 13 seem to indicate that it is experimentally trivial to distinguish between the two mechanisms because the A-1 rate does not depend on the concentration of nucleophile (water). However, epoxide hydrolysis reactions are typically carried out with water acting as both reactant and solvent and therefore its concentration effectively remains constant during the course of the reaction. Even in a purely A-2 mechanism, a pseudo second order rate constant is measured in the laboratory with water's concentration (55.5 M) being multiplied into the rate constant (see Equation 13). Other experimental and/or theoretical methods are required to assign the appropriate mechanism for a particular epoxide.

While both mechanisms are distinct and favorable under certain conditions, it is not straightforward to assign the reaction mechanism based solely on the structure of the epoxide. The solvent deuterium isotope effect has been used in previous studies to distinguish the reaction mechanism because the ratio of the rate constants in D₂O versus H₂O is calculated to be 1.0 for the A-2 mechanism and 2.1 for the A-1 mechanism.²⁸ However, values of the deuterium isotope effect (k_{D_2O}/k_{H_2O}) may vary greatly.^{16, 27} The stereochemistry of the final diol product may also distinguish between the two mechanisms because a racemic mixture is typically expected in the A-1 mechanism where a nucleophile may add above or below the plane of the carbocation while only anti addition occurs in the A-2 mechanism. These observables were used to attribute the A-2 mechanism to a majority of the epoxides studied by Eddingsaas *et al.*¹⁶ A recent theoretical study also predicted that the A-1 mechanism was the least likely pathway in the hydrolysis of substituted epoxides.²⁹ In this computational study, all the epoxides that were studied also exhibited characteristics consistent with the A-2 or 'borderline' A-2³⁰ mechanism as will be shown in the Results and Discussion section.

Computational Methods

All electronic structure calculations were performed using the *Gaussian 09* electronic structure program.³¹ Most calculations were carried out using a relatively new density functional M062x³² with the 6-311++G** basis set. More lengthy calculations that mapped entire reaction trajectories using the nudged elastic band method^{33, 34} involved a smaller basis set (6-31+G*) with the M062x density functional (see Supporting Information). In order to obtain the liquid phase standard free energies of reactants, transition states and products for epoxide ring opening reactions, hydrogen bonded molecular clusters were constructed and immersed in a dielectric continuum described by the SMD solvation model³⁵ to simulate the liquid phase. Molecular clusters have been shown to improve the accuracy of electronic structure calculations in the liquid phase because both short range intermolecular interactions (particularly in the first solvation shell) and long range electrostatics may be accounted for.³⁶ However, larger cluster sizes greatly increase the configuration space and computation time.³⁷ In this work, only small clusters containing the reactants and several additional water molecules are considered.

When conducting cluster calculations, the configuration space is typically sampled to find a minimum energy starting configuration. To commence the search, a cluster size needs to be determined. A minimum of four species are required to describe the entire hydrolysis reaction: an epoxide, an acid (typically H_3O^+), a nucleophilic water and another water molecule that receives the proton from the protonated diol after the addition reaction has occurred. The configuration space is restricted by requiring that the cluster is arranged in a reactive configuration. For epoxide hydrolysis, the acid is hydrogen bonded to the epoxide oxygen that it donates to while the nucleophilic water and proton receiving water molecule are placed below the plane defined by the epoxide C-C and epoxide-substituent C-R bonds. An additional water molecule was used to hydrogen bond with H_3O^+ was to obtain a stable reactant cluster geometry containing a neutral epoxide. Without it, the proton will

directly transfer to the epoxide as observed in other calculations of H_3O^+ hydrogen bonded to oxidized organics.³⁸ The resulting pentamer ($\text{H}_2\text{O} \cdots \text{H}_3\text{O}^+ \cdots \text{epoxide} \cdots \text{H}_2\text{O} \cdots \text{H}_2\text{O}$) therefore represented the simplest structure that served as a starting point for all cluster calculations. During preliminary optimizations, clusters would converge to a ring structure such as the one shown in Figure 2. The ring structure geometry consistently optimized for all clusters except an epoxide cluster containing SO_4^{2-} which gave rise to branched hydrogen bonded rings. In this case, two intermolecular distances were fixed in order to ensure that the cluster contained the same underlying structure so that comparisons may be made (see Supporting Information). As mentioned above, the cyclic structure represents a reactive configuration and is not the minimum energy configuration of the cluster in a dielectric continuum. A lower energy conformation may be realized if the H_3O^+ is allowed to explicitly hydrogen bond with three species (2 H_2O 's and the epoxide). This however would require several hydrogen bonds to break in order for a nucleophilic water to attack below the epoxide in the transition state giving rise to a relatively large barrier. While the reactive configuration is less stable because specific molecules are not explicitly solvated, so too is the transition state for the same reason which has somewhat of a canceling effect when calculating the reaction barriers. More accuracy may potentially be achieved by using larger clusters although at the cost of computational speed. The cyclic pentamer was therefore used in most reaction barrier calculations because it was computationally feasible and reasonably accurate in predicting rate constants as will be shown in the Results and Discussion.

The reactive cyclic cluster configuration shown in Figure 2 has several advantages. Firstly, calculations that use water as the acid (neutral aerosols) require a means to neutralize charge separated species to form stable products (OH^- from the H_2O that donated a proton to the epoxide oxygen is neutralized by the proton from R-OH_2^+ generated after nucleophilic attack via proton transfer through two water molecules). With two additional water molecules, a proton wire is formed³⁹ enabling the separated charges to be neutralized. Movie 1 in the Supporting Information displays this transfer for the

hydrolysis of oxirane in neutral water. Secondly, acidic species like H_3O^+ that are present in reactant and product complexes (above and below the epoxide ring respectively for anti addition) are partly solvated via a hydrogen bond to an adjacent water molecule in the ring structure. This may more accurately capture proton transfer dynamics which are known to involve water molecules in the first and second solvation shells.⁴⁰ For these reasons this cluster structure was used in all calculations to approximate the local solvation and reaction dynamics of epoxide reactions.

Equation 6 indicates that free energies have two terms that were independently calculated for each reaction studied. The pseudochemical potential energies (ΔG^*) were determined by optimizing the reactant, transition state and product clusters (fully associated) in a dielectric continuum as described above. Because all clusters were fully associated (i.e. separate reactant or product species were not optimized and were instead calculated as an associated complex), it was not necessary to locate and optimize the protonated epoxide intermediate for rate constant calculations because the overall barrier ($\Delta G_1 + \Delta G_2^\ddagger$) depends only on the free energy difference between the transition state and reactants (see Equations 11 and 15 and Figure 1). All stationary and saddle point geometries in addition to vibrational frequencies were optimized in the reaction field of the implicit solvent. All minima and transition states were confirmed to possess zero and one imaginary frequency respectively.

The second term in Equation 6 describing the entropy of liberation was approximated as follows. The reactant complex for every epoxide reaction was segregated into two reacting species: the epoxide and an acid/2 H_2O /nucleophile complex. Each of these species had entropies calculated according to Equation 4 whose sum was subtracted from the entropy of the fully associated transition state complex. The size of the reacting complexes (number of associated waters) affects the magnitude of $\Delta S_{lib,act}$ giving rise to systematic errors for this calculation. However, all optimized complexes

consistently contained two tightly bound water molecules so that relative rates are readily compared in rate constant calculations.

Results and Discussion

The simplest water soluble epoxide is oxirane. While volatile, it is miscible in water and its acid catalyzed hydrolysis rate was determined by Pritchard and coworkers.⁴¹ In that work, it was argued that acid catalyzed oxirane hydrolysis proceeds by an A-1 mechanism because the reaction follows the Zucker-Hammett acidity function.⁴² The Zucker-Hammett postulate however is not considered a strong indicator of reaction mechanism.⁴³ A contrasting view in which the A-2 mechanism is invoked to describe the hydrolysis of primary and secondary epoxides has been proposed.²⁷ Even tertiary epoxides, which are typically acknowledged to participate in the A-1 hydrolysis pathway because they can form stable tertiary carbocations have been speculated to partake in the A-2 mechanism.^{16, 27} While interpretation of a variety of experimental data may lead to differing conclusions, computational methods are capable of characterizing the structure of transition states so that less ambiguous assignments may be made. Such assignments are predicated on accurate models that are capable of reproducing experimental data. The aim of this work is not only to calculate empirically determined rate constants but to also predict the kinetics of novel atmospheric epoxides that have not been measured.

Figure 3 illustrates the reactant, transition state and product complexes for acid catalyzed oxirane hydrolysis that were optimized in a water dielectric continuum. For this reaction, a protonated oxirane intermediate was not found. This may be a consequence of the small water clusters used in these simulations that do not incorporate complete first and second solvation shells where important hydrogen bond dynamics may stabilize such transient species.⁴⁴ Interestingly, protonated organic oxides have been observed in gas phase calculations of an H_3O^+ -carbonyl complex (containing no additional water molecules) indicating that dissociation of hydrogen bonds within the first solvation shell may be

important.³⁸ Additionally, a carbocation intermediate was not found for oxirane. Instead, Figure 3b depicts a transition state where the epoxide ring is partly open, a partial inversion of stereochemistry is occurring at the epoxide carbon, and a water molecule (nucleophile) is interacting with the same epoxide carbon where it is adding in an anti fashion. The deviation from planarity at the epoxide carbon being attacked in the transition state is 8.7° indicating that considerable inversion of stereochemistry has already occurred. These observations are consistent with an A-2 mechanism for oxirane.

Figure 3 does not display the protonated epoxide intermediate that is expected to form prior to the ring opened transition state. As described above, with this cluster and at this level of theory, the intermediate was not found to be a stationary state. This is evident in Figure 4 which displays a plot of the minimum energy pathway on a simplified pseudochemical potential energy surface (no zero point vibrational energy corrections) for the acid catalyzed hydrolysis of oxirane. The NEB calculation looks similar to the schematic free energy surface of the A-2 mechanism in Figure 1 although there are no pronounced protonated intermediates (local minima). Despite this, the NEB result displayed in Figure 4 may be used to approximate the pK_a of a protonated epoxide. From Figure 4, the pseudochemical potential energy difference between the protonated epoxide + water versus the epoxide + hydronium ion is approximately -3.8 kcal/mol. The change in the entropy of liberation (see Equation 6) between the reactant and product species is negligible because only a proton of small mass is transferred. Therefore, the approximate free energy difference is also -3.8 kcal/mol. Using the relationship of $K_a = \exp(\Delta G/RT)$, the pK_a is estimated to be -2.8 at 298 K for a protonated epoxide. This agrees very well with $pK_a \sim -2.5$ for protonated ethers.⁴⁵ The overall reaction barrier may then be used to compute the rate constant for oxirane. At the M062x/6-311++G** level, $\Delta G^* = 15.4$ kcal/mol (zero point energy corrected). The addition of another water molecule to the reactant cluster at the site of the epoxide oxygen did not cause a substantial change in the pseudochemical potential energy barrier ($\Delta G^* = 14.7$ kcal/mol; see Supporting Information). This further supported the use of only five molecules in cluster

calculations as described in the previous section and shown in Figure 2. $\Delta S_{\text{lib}} = 7.3$ kcal/mol which gives a third order rate constant of $k_{\text{oxirane, 3rd}} = 1.4\text{e-}4 \text{ M}^{-2}\text{s}^{-1}$ using Equation 15 with an A-2 mechanism. Because water is acting as both nucleophile and solvent, the pseudo second order rate constant for oxirane is determined to be $k_{\text{oxirane, 2nd}} = (55.5 \text{ M}) * k_{\text{oxirane, 3rd}} = 7.7\text{e-}3 \text{ M}^{-1}\text{s}^{-1}$. This calculation also agrees very well with the measured rate constant of $9\text{e-}3$ for oxirane.⁴² The model therefore captures essential proton transfer and ring opening reaction dynamics in acid catalyzed reactions of simple epoxides such as oxirane.

To what extent does the presence and identity of the acid affect the reaction barrier for epoxide hydrolysis? Figure 2 in the paper by Long and Pritchard⁴¹ indicates that the first order rate constant (where the H^+ concentration has been multiplied with the 2nd order rate constant: $k_{1\text{st}} = k_{2\text{nd}}[\text{H}^+]$) increases rapidly as the H^+ concentration decreases several pH units for isobutylene hydrolysis. In this work, the affect of the acid on the reaction barrier was calculated for oxirane hydrolysis for three different cases: neutral (H_2O), hydronium ion (H_3O^+), and formic acid (HCOOH). Formic acid was selected because it is the smallest carboxylic acid that represents the class of weak organic acids in aerosol particles. Figure 5 shows the FESs for all three reactions. It is readily evident that acids, particularly strong acids like H_3O^+ , greatly influence the reaction barrier by making the epoxide ring more susceptible to opening. For oxirane, a weak acid lowers the overall activation free energy by 7.5 kcal/mol while a strong acid lowers it by 13.5 kcal/mol. These effects are significant considering that they are comparable to some enzymes.^{46, 47} The difference in epoxide reactivity when strong acids (versus weak acids) are used is also notable and is a consequence of an equilibrium that favors higher protonated epoxide concentrations (K_1 is larger for reactions involving H_3O^+ than HCOOH in Equation 14). The calculations therefore predict that the role of organic acids in catalyzing epoxide ring opening reactions in aerosol particles is limited, particularly in the presence of stronger inorganic acids such as H_2SO_4 and HNO_3 that dissociate and form H_3O^+ in the presence of water. Without an acid present, the mechanism

of epoxide hydrolysis is fundamentally different. In this case, proton transfers that neutralize all charged species in the cluster occur subsequent to epoxide ring opening. This is more clearly illustrated in three different movies (see Supporting Information) depicting the minimum energy pathway of oxirane hydrolysis using water (H_2O), hydronium ion (H_3O^+), and formic acid (HCOOH) respectively. In the cases involving acids, the H_3O^+ and HCOOH are regenerated illustrating the catalytic effect. All cases are also consistent with an A-2 mechanism where the attacking water molecule is interacting with the epoxide carbon whose bond is breaking with the epoxide oxygen in the transition state.

As mentioned at the beginning of this section, the A-2 mechanism accounts for the hydrolysis of simple primary and secondary epoxides. For tertiary epoxides, there is a general tendency to ascribe an A-1 mechanism²⁷ because a tertiary carbocation intermediate may form. While tertiary carbocations are more stable than primary or secondary carbocations,⁴⁸ this does not imply that tertiary epoxides will always hydrolyze via the A-1 pathway because it may still possess a barrier that is greater than an A-2 pathway. To examine this further, calculations were performed to try and isolate a tertiary carbocation intermediate derived from isobutylene oxide (2-methyl-1,2-epoxypropane). 2 water molecules were placed above and below the plane of the carbocation to try and stabilize it. Several iterations of placing the water molecules at different distances from the carbocation always resulted in the formation of the protonated alcohol adduct (see Supporting Information). This result along with stereochemical evidence²⁷ and kinetic isotope effects for tertiary epoxides that resemble IEPOX¹⁶ have led us to ascribe an A-2 mechanism for all epoxides studied in this paper. This has important implications in aerosol chemistry because the reaction rate depends on the concentration of the nucleophile (see Equation 13). While the concentration of water is not a variable in laboratory experiments because it is the solvent, the same cannot be stated for aerosol particles that consist of a variety of organic and inorganic compounds mixed with water whose concentration may vary. Water's aerosol concentration therefore

has to be taken into account and third order rate constants need to be used if this chemistry is to be incorporated into an atmospheric model.

While oxirane is not considered to play a major role in SOA formation, the techniques and analysis just described were applied to the study of a series of epoxides including two recently discovered atmospheric epoxides: IEPOX and MAE. Both epoxides are produced from the oxidation of isoprene under low and high NO_x conditions respectively. Table 1 contains a list of 10 epoxides, activation free energies and acid catalyzed hydrolysis rate constants calculated using H_3O^+ as the acid. Structural atomic coordinates, zero point corrected energies and vibrational frequencies for all reactants, transition states and products of Table 1 are listed in the Supporting Information. 7 of the epoxides (including β -IEPOX and MAE) are asymmetric and therefore require rate constants to be computed for nucleophilic attack on either carbon of the epoxide ring. Of the 7, rate constants for three epoxides were computed for nucleophilic attack at both carbons (2,3-epoxypropan-1-ol, β -IEPOX and MAE). It is evident from Table 1 that epoxide hydrolysis occurs at the less substituted site for 2,3-epoxypropan-1-ol and MAE while it occurs at the more substituted site for IEPOX. For 2,3-epoxypropan-1-ol and β -IEPOX, the larger rate constant is to be compared with the measured value because its pathway is kinetically more favorable. The other four epoxides (1,2-epoxypropane, 2-methyl-1,2-epoxypropane, 2-methyl-2,3-epoxypropan-1-ol, 2,3-epoxypropanoic acid) possess a primary carbon site that appears like oxirane to a nucleophile. Attack at the primary site for 2,3-epoxypropan-1-ol and MAE yielded rate constants similar to oxirane and therefore the rate constants for reactions at the primary site in the other four epoxides are also assumed to be similar to oxirane and were not computed as a result.

Table 1 contains the changes in pseudochemical potential energies (ΔG^*), the free energies of liberation ($-T\Delta S$) and the free energies of activation (ΔG_{act}^0) calculated according to Equation 6. The

free energies of activation were then used to calculate third order rate constants using Equation 15 (A-2 mechanism). The third order rate constants were converted to pseudo second order rate constants by multiplication with the water concentration (55.5 M) so that the computational results may be directly compared with experiments.^{16, 41, 49, 50} The measured and calculated second order rate constants are displayed in Figure 6. The calculated rate constants are in excellent agreement with available experimental data for small epoxides such as oxirane and 1,2-epoxypropane. Overestimates tend to occur for larger and more oxygenated epoxides including IEPOX. In these cases, the average barrier height underestimation is approximately 2 kcal/mol. It is difficult to determine the major source(s) of uncertainty in this model calculation because numerous approximations have been made. The level of theory in the electronic structure calculations, lack of configuration space sampling, small water cluster size, solvation model, and the simplified transition state theory rate constant expression may all affect the accuracy of the results. Additionally, the assignment of a purely A-2 mechanism for tertiary epoxides such as 2-methyl-2,3-epoxypropan-1-ol and β -IEPOX may be inaccurate because the transition states exhibit borderline A-2 character with a larger intermolecular distances (> 2.5 Angstroms) computed between the ring opened epoxide and the attacking nucleophile relative to primary and secondary epoxides (see Supporting Information). In such borderline cases, concurrent A-1 and A-2 mechanisms may be required to describe the reaction rate.³⁰

Even with all the model approximations, the calculations capture the appropriate trends of acid catalyzed epoxide hydrolysis observed in experimental studies.¹⁶ Namely, electron donating groups (such as $-\text{CH}_3$) that are bonded to the carbon being attacked by water stabilize the transition state and therefore increase the reaction rate. Electron withdrawing groups (such as $-\text{CH}_2\text{OH}$ and $-\text{COOH}$) exhibit the converse effect and therefore decrease the reaction rate. The effect is most pronounced with epoxides containing carboxylic acid groups whose rate constants are at least several orders of magnitude smaller than less oxygenated epoxides. This effect ensures that only one stereoisomer is

favorable for the hydrolysis of β -IEPOX and MAE. For β -IEPOX, the water bonds with the tertiary carbon while for MAE it bonds with the primary carbon because the other stereoisomer forms considerably slower (see Table 1). Structurally, the transition states of β -IEPOX and MAE are also different as shown in Figure 7. For MAE, the oxygen from the epoxide ring and the attacking water molecule are interacting more closely with the epoxide carbon than for β -IEPOX. The combination of the ring strain and the strong inductive effects from the -COOH group destabilizing the partially positively charged epoxide carbon atom are contributing factors to MAE's higher barrier (smaller rate constant). While there are no published hydrolysis rate constants for MAE, the calculations here may be used to predict its rate constant. Considering that MAE is oxygenated, the calculations may over-estimate the rate constant like they do for β -IEPOX assuming that the empirical rate constant is correct. However, MAE hydrolyzes at the primary carbon site which appears like oxirane and its calculated rate constant is similar to that of oxirane (within a factor of 5 or a 0.9 kcal/mol difference in barrier height). This suggests that the calculations may not overestimate the rate constant because they are accurate for oxirane. In this case, β -IEPOX ($k = 5\text{E-}2 \text{ M}^{-1}\text{s}^{-1}$)¹⁶ hydrolyzes ~30 times faster than MAE ($k = 1.7\text{E-}3 \text{ M}^{-1}\text{s}^{-1}$). These results suggest that if both IEPOX and MAE are present in the atmosphere, IEPOX will hydrolyze more readily to form methyltetrols compared with MAE forming methylglyceric acid. Despite these results, both compounds are known isoprene tracers that have been detected in ambient aerosols.⁸

While hydrolysis reactions for atmospherically generated epoxides are favorable in acidic aerosols, other competitive epoxide reactions may also occur in particles containing inorganic and organic compounds. Sulphate, nitrate and alcohols may also act as nucleophiles in acid catalyzed epoxide ring opening reactions to form organosulfates, organonitrates and oligomers. By calculating the rate constants for representative reactions involving different nucleophiles, the branching ratios may be determined. This information is crucial to modeling the complex chemistry occurring in ambient aerosol particles.

Table 2 displays the calculated third order rate constants for epoxide reactions with H_2O , SO_4^{2-} , NO_3^- , $\text{CH}_3\text{CH}_2\text{CH}_2\text{OH}$ and $\text{HOCH}_2\text{CH}_2\text{CH}_2\text{OH}$. Propanol and 1,3-propanediol were selected to represent larger organic alcohols (such as methyltetrols) that may be present in the aerosol. If only considering H_2O , SO_4^{2-} , NO_3^- , and $\text{HOCH}_2\text{CH}_2\text{CH}_2\text{OH}$, the branching ratios are 0.07, 0.70, 0.01 and 0.22 respectively. If all nucleophile concentrations were equivalent, the calculations predict that epoxides would most readily produce organosulfate compounds in acidic aerosols. However, concentrations in aerosols are variable and hydrolysis reactions are competitive even in drier aerosols given the small molecular weight of water. Organonitrates are least likely to form because NO_3^- represents a weaker nucleophile relative to H_2O .¹⁶ These results are consistent with recent experimental work by Darer et al. that observed more facile nucleophilic substitution of water with organonitrates relative to organosulfates.⁵¹ In contrast, oligomerization reactions⁵² represent another significant pathway for epoxides particularly in dry aerosols. Dimers and higher order oligomers may be produced by the addition of another epoxide to the growing chain. Dommen *et al.*⁵³ have observed such species in laboratory experiments involving isoprene. Polymers of methylglyoxal and similar compounds have been observed in other experiments.⁵⁴ These reactions naturally decrease the volatility of the organic matter by producing larger compounds and their impact on SOA formation and growth is significant based on the calculations presented here.

One final consideration that warrants discussion in the computational model is the dielectric continuum. The choice of continuum solvent will affect the solvation of the reactant and transition state molecular complexes. By varying the dielectric continuum, the solvation of different states along the reaction coordinate may be differentially impacted thereby influencing the barrier height of the reaction. In order to examine the influence of the continuum on the rate constants, three different calculations of the hydrolysis of IEPOX were carried out using water, ethanol and *n*-octanol as continuum solvents. These solvents were selected because they represent a wide range of polarity.

Table 3 displays the reaction barriers and rate constants of IEPOX in the three different continuum solvents. As the polarity of the solvent decreases, there is a decrease in the barrier height with a resultant increase of the hydrolysis rate constant. Solvent polarity therefore may play an important role in modulating barrier heights of reactions in aerosols.

These calculations raise critical issues that are typically overlooked in atmospheric aerosol models. While gas phase compounds and reaction rates may be measured with good precision and accuracy, the same cannot be stated for aerosol phase reactions. Aerosol phase reaction kinetics may only be approximated in the laboratory using pure solvents or simple mixtures. Such studies therefore do not account for aerosol chemical and phase heterogeneity in addition to surface effects. Many of these effects may be modeled using computational chemistry which will provide valuable insight in describing ambient aerosol reactors.

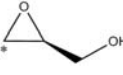
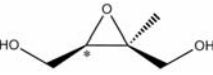
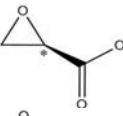
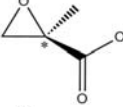
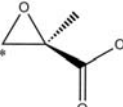
Conclusions

Density functional theory was applied to study acid catalyzed epoxide ring opening reactions of atmospherically relevant epoxides. In aerosols derived from isoprene SOA, the hydrolysis of IEPOX proceeds approximately 30 times faster than MAE. Strong acids (like H_3O^+) and strong nucleophiles (like SO_4^{2-}) considerably lower the overall reaction barrier. Additionally, oligomerization reactions are at least as reactive as water with epoxides indicating that this pathway is important in dry aerosols. Further experimental and computational studies are poised to decipher other important reactive pathways occurring within ambient aerosol particles.

Acknowledgements

The authors thank Dr. Nicole M. Deschamps for useful discussions. The US Environmental Protection Agency through its Office of Research and Development collaborated in the research described here. It has been subjected to the Agency's administrative review and approved for publication. Although this work was reviewed by EPA and approved for publication, it may not necessarily reflect official agency policy. Mention of trade names or commercial products does not constitute endorsement or recommendation for use.

Table 1. Calculated and measured acid catalyzed epoxide hydrolysis rate constants in water.

Epoxide	ΔG^\ddagger	$-T\Delta S_{lib}^\ddagger$	ΔG_{act}°	$k_{calc} (M^{-2}s^{-1})$	$k_{calc} (M^{-1}s^{-1})$	$k_{meas} (M^{-1}s^{-1})$	
1. oxirane		15.4	7.3	22.7	1.4E-04	8.0E-03	9.0E-03 ^a
2. 1,2-epoxypropane (secondary carbon)		14.0	7.5	21.5	1.1E-03	5.9E-02	6.0E-02 ^a
3. 2-methyl-1,2-epoxypropane (tertiary)		9.7	7.6	17.2	1.5E+00	8.2E+01	6.8E+00 ^a
4. <i>cis</i> -2,3-epoxybutane		13.4	7.6	20.9	2.7E-03	1.5E-01	2.0E-01 ^b
5a. 2,3-epoxypropan-1-ol (secondary)		16.6	7.6	24.2	1.2E-05	6.6E-04	
5b. 2,3-epoxypropan-1-ol (primary)		14.6	7.6	22.2	3.2E-04	1.8E-02	2.5E-03 ^c
6. 2-methyl-2,3-epoxypropan-1-ol (tertiary)		11.6	7.6	19.2	5.1E-02	2.8E+00	1.1E-02 ^c
7. <i>cis</i> -2,3-epoxybutane-1,4-diol		14.9	7.7	22.6	1.6E-04	8.7E-03	1.3E-03 ^b 1.4E-03 ^d
8a. 2-methyl-2,3-epoxybutan-1,4-diol (β -IEPOX, tertiary)		11.4	7.7	19.2	5.3E-02	2.9E+00	5.0E-02 ^b 3.6E-02 ^d
8b. 2-methyl-2,3-epoxybutan-1,4-diol (β -IEPOX, secondary)		13.8	7.7	21.6	9.0E-04	5.0E-02	
9. 2,3-epoxypropanoic acid (secondary)		21.4	7.6	29.0	3.1E-09	1.7E-07	
10a. 2-methyl-2,3-epoxypropanoic acid (MAE, tertiary)		21.1	7.7	28.8	4.6E-09	2.5E-07	
10b. 2-methyl-2,3-epoxypropanoic acid (MAE, primary)		15.9	7.7	23.6	3.0E-05	1.7E-03	

All free energy terms are in kcal/mol.

* denotes the carbon that bonds with H₂O (nucleophile) in the calculation.

^a Values from Long *et al.*⁴¹

^b Values from Eddingsaas *et al.*¹⁶

^c Values from Mabey *et al.*⁵⁰

^d Values from Cole-Filipiak *et al.*⁴⁹

Table 2. Calculated rate constants (3rd order) for the acid catalyzed β -IEPOX ring opening reactions with different nucleophiles in a water dielectric continuum.

Nucleophile	ΔG^*	$-T\Delta S_{lib}$	ΔG_{act}^0	$k_{calc} (M^{-2}s^{-1})$
H ₂ O	11.4	7.7	19.2	5.3E-02
SO ₄ ²⁻	9.7	8.1	17.8	5.2E-01
NO ₃ ⁻	12.3	8.0	20.3	7.6E-03
CH ₃ CH ₂ CH ₂ OH	10.4	8.0	18.4	1.9E-01
HOCH ₂ CH ₂ CH ₂ OH	10.5	8.0	18.5	1.6E-01

Table 3. Calculated rate constants (3rd order) for the acid catalyzed hydrolysis of β -IEPOX using different continuum solvents.

Continuum Solvent	$\epsilon (20^\circ C)$	ΔG_{act}^0 (kcal/mol)	$k_{calc} (M^{-2}s^{-1})$
water	80.4	19.2	5.3E-02
ethanol	25.6	17.1	1.6E+00
<i>n</i> -octanol	10.3	15.6	2.2E+01

Figure Captions

Figure 1. Schematic free energy surfaces for the a) A-1 and b) A-2 mechanisms of epoxide hydrolysis.

Figure 2. Cyclic oxirane- H_3O^+ -water cluster optimized in a H_2O dielectric continuum.

Figure 3. Reactant, transition state and product oxirane reaction clusters optimized in a H_2O dielectric continuum. The hydrolysis proceeds with an H_3O^+ catalyst that is regenerated.

Figure 4. Nudged elastic band (NEB) calculation (M062x/6-31+G*) of the minimum pseudochemical potential (G^*) energy path for the acid catalyzed hydrolysis of oxirane.

Figure 5. Free energy barriers for the hydrolysis of oxirane using H_2O , H_3O^+ and HCOOH as acids. The stronger the acid, the lower the hydrolysis free energy barrier.

Figure 6. Second order rate constant measurements and calculations (at the more and less substituted carbon positions) for a series of 10 epoxides including β -IEPOX and MAE.

Figure 7. Transition state structures of the acid catalyzed hydrolysis of a) β -IEPOX and b) MAE.

Figure 1.

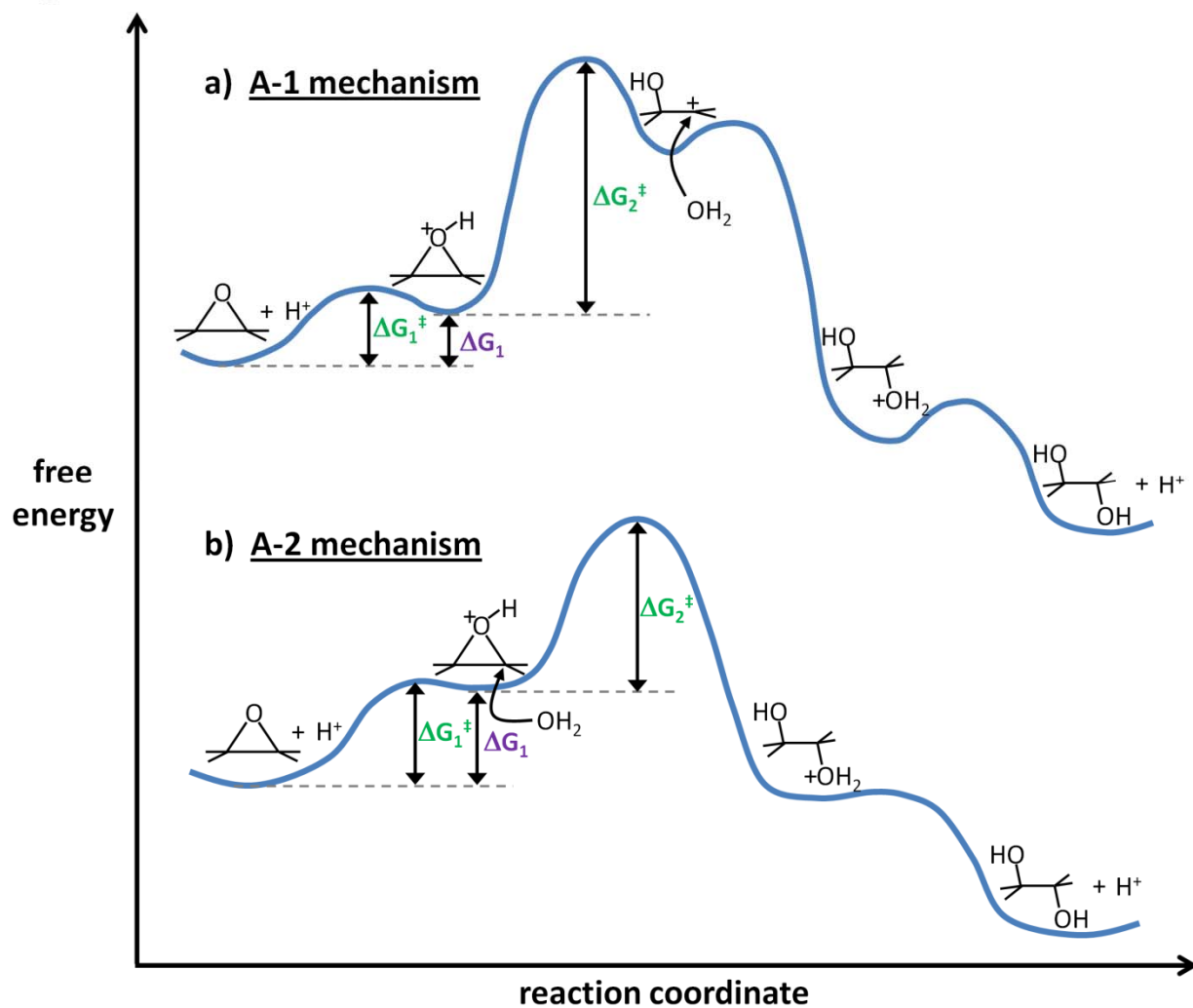


Figure 2.

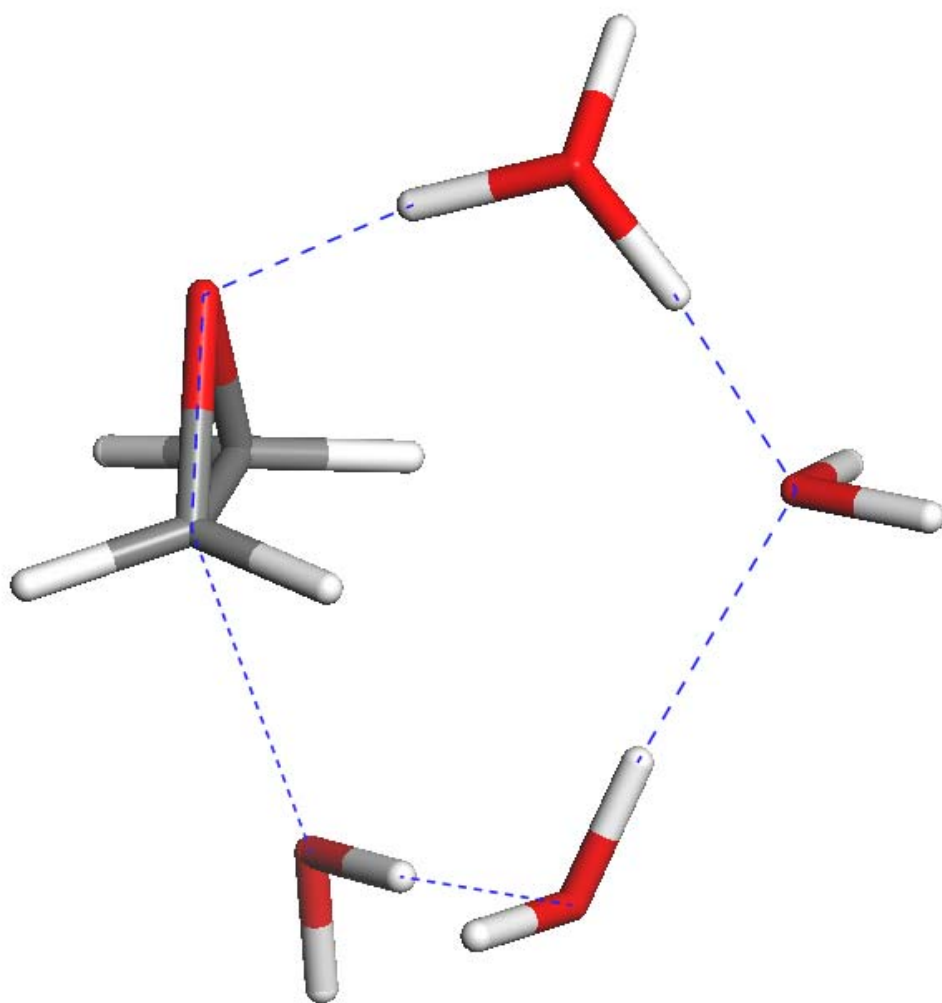


Figure 3.

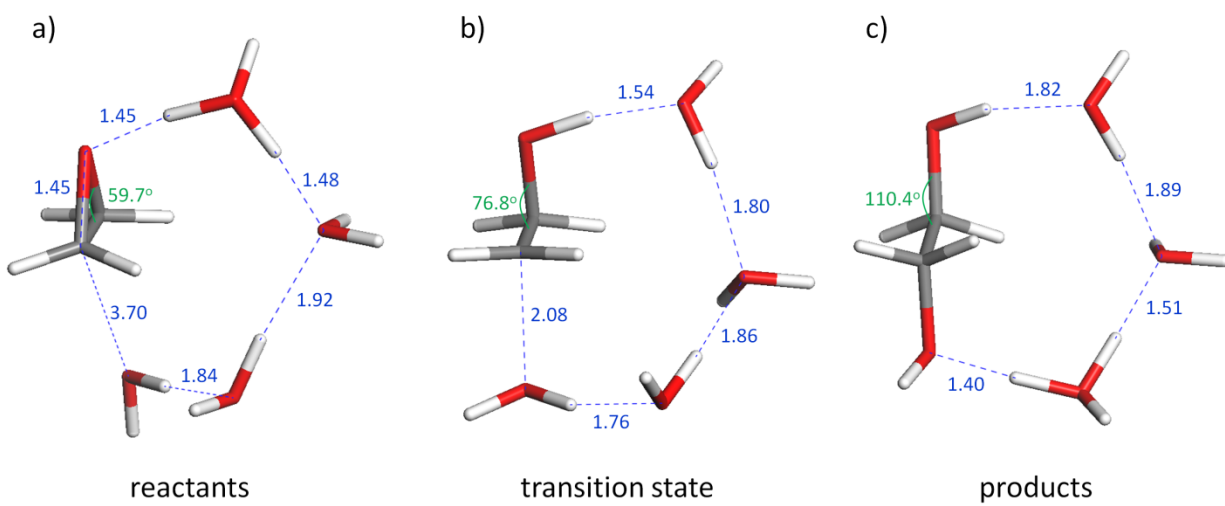


Figure 4.

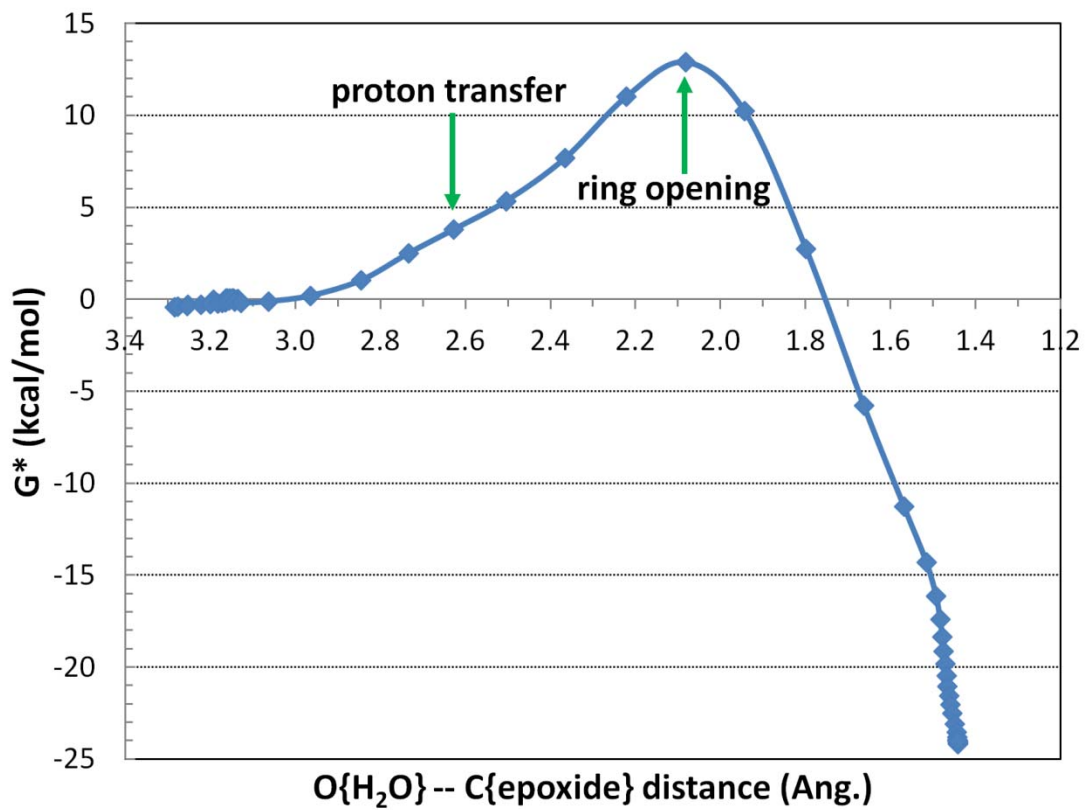


Figure 5.

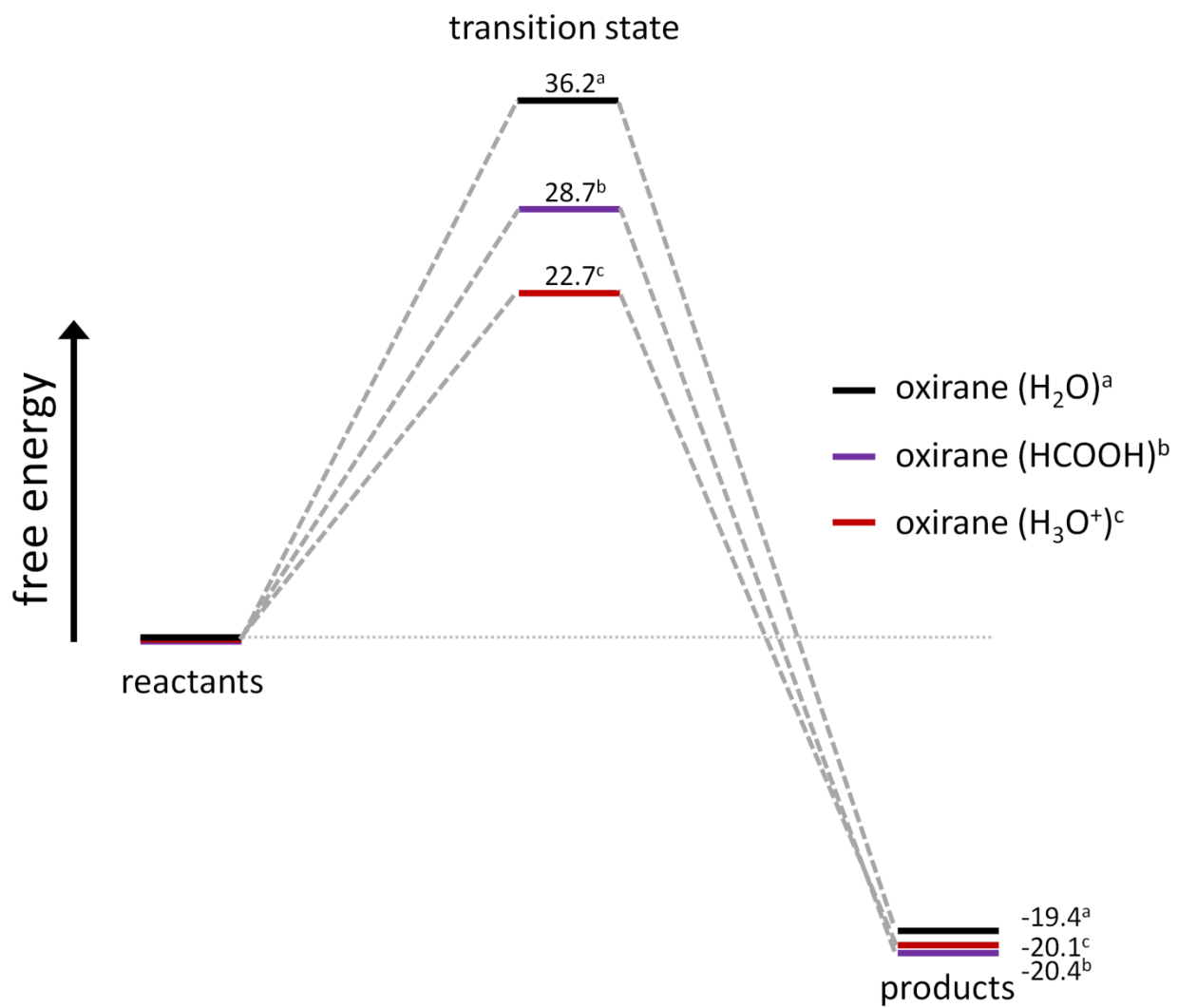


Figure 6.

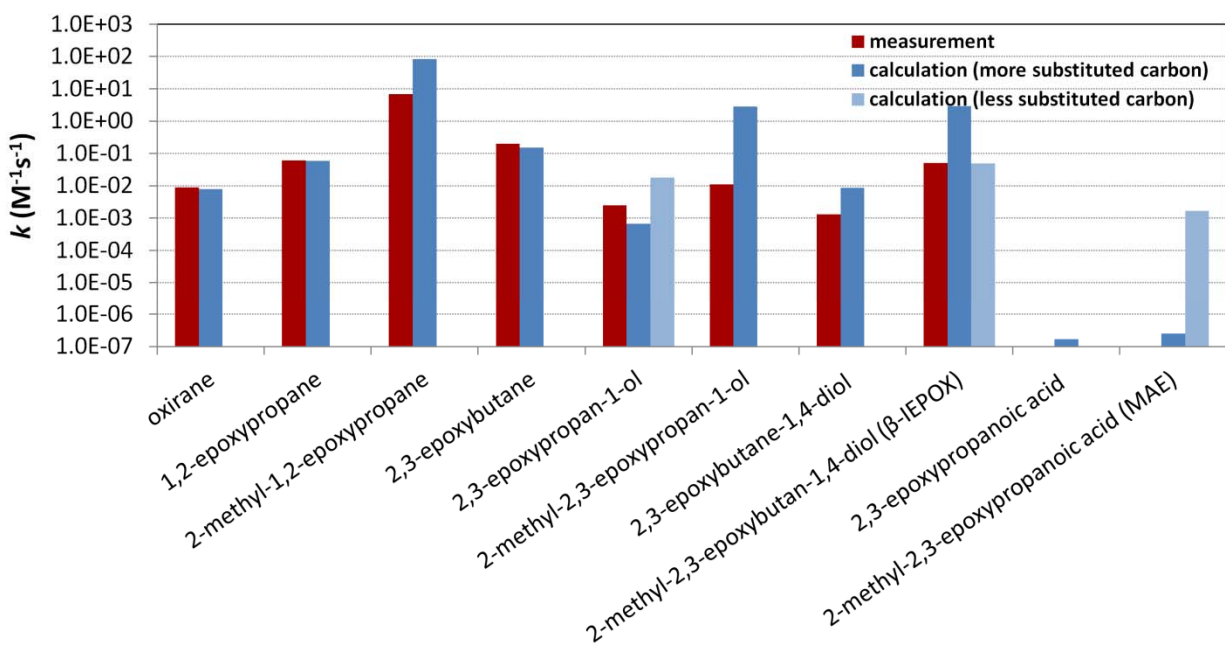
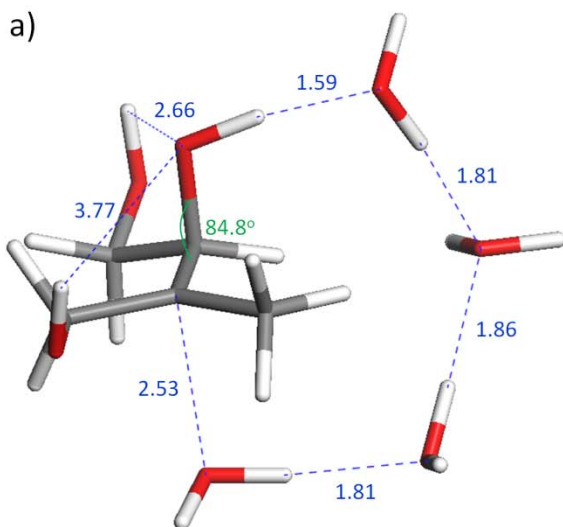
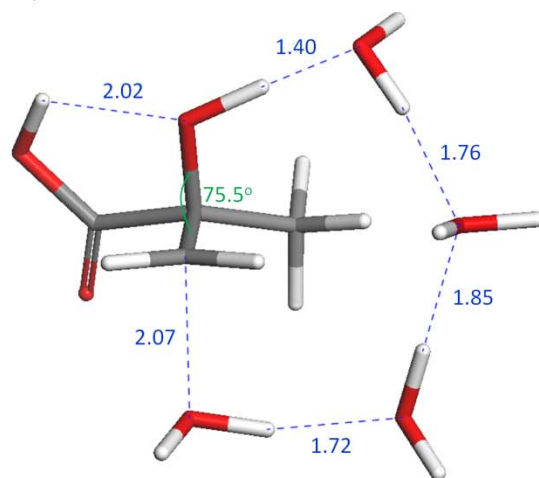


Figure 7.

a)



b)



References

1. R. D. Brook, S. Rajagopalan, C. A. Pope, III, J. R. Brook, A. Bhatnagar, A. V. Diez-Roux, F. Holguin, Y. Hong, R. V. Luepker, M. A. Mittleman, A. Peters, D. Siscovick, S. C. Smith, Jr., L. Whitsel, J. D. Kaufman, E. Amer Heart Assoc Council, D. Council Kidney Cardiovasc and M. Council Nutr Phys Activity, *Circulation*, 2010, **121**, 2331-2378.
2. J. E. Hart, E. Garshick, D. W. Dockery, T. J. Smith, L. Ryan and F. Laden, *Am. J. Respir. Crit. Care Med.*, 2011, **183**, 73-78.
3. T. L. Anderson, R. J. Charlson, S. E. Schwartz, R. Knutti, O. Boucher, H. Rodhe and J. Heintzenberg, *Science*, 2003, **300**, 1103-1104.
4. Q. Zhang, J. L. Jimenez, M. R. Canagaratna, J. D. Allan, H. Coe, I. Ulbrich, M. R. Alfarra, A. Takami, A. M. Middlebrook, Y. L. Sun, K. Dzepina, E. Dunlea, K. Docherty, P. F. DeCarlo, D. Salcedo, T. Onasch, J. T. Jayne, T. Miyoshi, A. Shimono, S. Hatakeyama, N. Takegawa, Y. Kondo, J. Schneider, F. Drewnick, S. Borrmann, S. Weimer, K. Demerjian, P. Williams, K. Bower, R. Bahreini, L. Cottrell, R. J. Griffin, J. Rautiainen, J. Y. Sun, Y. M. Zhang and D. R. Worsnop, *Geophysical Research Letters*, 2007, **34**.
5. J. L. Jimenez, M. R. Canagaratna, N. M. Donahue, A. S. H. Prevot, Q. Zhang, J. H. Kroll, P. F. DeCarlo, J. D. Allan, H. Coe, N. L. Ng, A. C. Aiken, K. S. Docherty, I. M. Ulbrich, A. P. Grieshop, A. L. Robinson, J. Duplissy, J. D. Smith, K. R. Wilson, V. A. Lanz, C. Hueglin, Y. L. Sun, J. Tian, A. Laaksonen, T. Raatikainen, J. Rautiainen, P. Vaattovaara, M. Ehn, M. Kulmala, J. M. Tomlinson, D. R. Collins, M. J. Cubison, E. J. Dunlea, J. A. Huffman, T. B. Onasch, M. R. Alfarra, P. I. Williams, K. Bower, Y. Kondo, J. Schneider, F. Drewnick, S. Borrmann, S. Weimer, K. Demerjian, D. Salcedo, L. Cottrell, R. Griffin, A. Takami, T. Miyoshi, S. Hatakeyama, A. Shimono, J. Y. Sun, Y. M. Zhang, K. Dzepina, J. R. Kimmel, D. Sueper, J. T. Jayne, S. C. Herndon, A. M. Trimborn, L. R. Williams, E. C. Wood, A. M. Middlebrook, C. E. Kolb, U. Baltensperger and D. R. Worsnop, *Science*, 2009, **326**, 1525-1529.
6. J. H. Kroll, N. L. Ng, S. M. Murphy, R. C. Flagan and J. H. Seinfeld, *Environmental Science & Technology*, 2006, **40**, 1869-1877.
7. A. G. Carlton, R. W. Pinder, P. V. Bhave and G. A. Pouliot, *Environmental Science & Technology*, 2010, **44**, 3376-3380.
8. E. O. Edney, T. E. Kleindienst, M. Jaoui, M. Lewandowski, J. H. Offenberg, W. Wang and M. Claeys, *Atmospheric Environment*, 2005, **39**, 5281-5289.
9. J. D. Surratt, S. M. Murphy, J. H. Kroll, a. L. N. Ng, L. Hildebrandt, A. Sorooshian, R. Szmigielski, R. Vermeylen, W. Maenhaut, M. Claeys, R. C. Flagan and J. H. Seinfeld, *Journal of Physical Chemistry A*, 2006, **110**, 9665-9690.
10. J. D. Surratt, J. H. Kroll, T. E. Kleindienst, E. O. Edney, M. Claeys, A. Sorooshian, N. L. Ng, J. H. Offenberg, M. Lewandowski, M. Jaoui, R. C. Flagan and J. H. Seinfeld, *Environmental Science & Technology*, 2007, **41**, 517-527.
11. F. Paulot, J. D. Crouse, H. G. Kjaergaard, A. Kurten, J. M. St Clair, J. H. Seinfeld and P. O. Wennberg, *Science*, 2009, **325**, 730-733.
12. Y.-H. Lin, H. Zhang, H. O. T. Pye, Z. Zhang, W. J. Marth, S. Park, M. Arashiro, T. Cui, S. H. Budisulistiorini, K. G. Sexton, W. Vizuete, Y. Xie, D. J. Luecken, I. R. Piletic, E. O. Edney, L. J. Bartolotti, A. Gold and J. D. Surratt, *Proceedings of the National Academy of Sciences of the United States of America*, 2013, **110**, 6718-6723.
13. T. Wang, Z. Liu, W. Wang and M. Ge, *Atmospheric Environment*, 2012, **56**, 58-64.

14. Y.-H. Lin, Z. Zhang, K. S. Docherty, H. Zhang, S. H. Budisulistiorini, C. L. Rubitschun, S. L. Shaw, E. M. Knipping, E. S. Edgerton, T. E. Kleindienst, A. Gold and J. D. Surratt, *Environmental Science & Technology*, 2012, **46**, 250-258.
15. E. C. Minerath, M. P. Schultz and M. J. Elrod, *Environmental Science & Technology*, 2009, **43**, 8133-8139.
16. N. C. Eddingsaas, D. G. VanderVelde and P. O. Wennberg, *Journal of Physical Chemistry A*, 2010, **114**, 8106-8113.
17. C. J. Cramer and D. G. Truhlar, *Chemical Reviews*, 1999, **99**, 2161-2200.
18. Y. J. Cho, S. R. Vandelinde, L. Zhu and W. L. Hase, *Journal of Chemical Physics*, 1992, **96**, 8275-8287.
19. S. Hammes-Schiffer and J. C. Tully, *Journal of Chemical Physics*, 1994, **101**, 4657-4667.
20. R. H. Zhou, *Proteins-Structure Function and Genetics*, 2003, **53**, 148-161.
21. C. P. Kelly, C. J. Cramer and D. G. Truhlar, *Journal of Physical Chemistry A*, 2006, **110**, 2493-2499.
22. D. A. McQuarrie, *Statistical Mechanics*, Harper & Row, New York, 1973.
23. A. Bennaïm, *Journal of Physical Chemistry*, 1978, **82**, 792-803.
24. A. Bennaïm and Y. Marcus, *Journal of Chemical Physics*, 1984, **81**, 2016-2027.
25. Y. Kim, J. R. Mohrig and D. G. Truhlar, *Journal of the American Chemical Society*, 2010, **132**, 11071-11082.
26. J. A. Miller and S. J. Klippenstein, *Journal of Physical Chemistry A*, 2006, **110**, 10528-10544.
27. D. L. Whalen, in *Advances in Physical Organic Chemistry, Vol 40*, ed. J. P. Richard 2005, vol. 40, pp. 247-298.
28. C. A. Bunton and V. J. Shiner, *Journal of the American Chemical Society*, 1961, **83**, 3207-3214.
29. R. C. Dantas Muniz Filho, S. A. Alves de Sousa, F. d. S. Pereira and M. M. Castro Ferreira, *Journal of Physical Chemistry A*, 2010, **114**, 5187-5194.
30. T. B. Phan, C. Nolte, S. Kobayashi, A. R. Ofial and H. Mayr, *Journal of the American Chemical Society*, 2009, **131**, 11392-11401.
31. M. J. Frisch, G. W. Trucks, H. B. Schlegel, G. E. Scuseria, M. A. Robb, J. R. Cheeseman, G. Scalmani, V. Barone, B. Mennucci, G. A. Petersson, H. Nakatsuji, M. Caricato, X. Li, H. P. Hratchian, A. F. Izmaylov, J. Bloino, G. Zheng, J. L. Sonnenberg, M. Hada, M. Ehara, K. Toyota, R. Fukuda, J. Hasegawa, M. Ishida, T. Nakajima, Y. Honda, O. Kitao, H. Nakai, T. Vreven, J. A. Montgomery Jr., J. E. Peralta, F. Ogliaro, M. Bearpark, J. J. Heyd, E. Brothers, K. N. Kudin, V. N. Staroverov, R. Kobayashi, J. Normand, K. Raghavachari, A. Rendell, J. C. Burant, S. S. Iyengar, J. Tomasi, M. Cossi, N. Rega, J. M. Millam, M. Klene, J. E. Knox, J. B. Cross, V. Bakken, C. Adamo, J. Jaramillo, R. Gomperts, R. E. Stratmann, O. Yazyev, A. J. Austin, R. Cammi, C. Pomelli, J. W. Ochterski, R. L. Martin, K. Morokuma, V. G. Zakrzewski, G. A. Voth, P. Salvador, J. J. Dannenberg, S. Dapprich, A. D. Daniels, O. Farkas, J. B. Foresman, J. V. Ortiz, J. Cioslowski and D. J. Fox, Gaussian, Inc., Wallingford CT, Revision A.1 edn., 2009.
32. Y. Zhao and D. G. Truhlar, *Chemical Physics Letters*, 2011, **502**, 1-13.
33. G. Henkelman and H. Jonsson, *Journal of Chemical Physics*, 2000, **113**, 9978-9985.
34. G. Henkelman, B. P. Uberuaga and H. Jonsson, *Journal of Chemical Physics*, 2000, **113**, 9901-9904.
35. A. V. Marenich, C. J. Cramer and D. G. Truhlar, *Journal of Physical Chemistry B*, 2009, **113**, 6378-6396.
36. Q. Cui, *Journal of Chemical Physics*, 2002, **117**, 4720-4728.
37. J. A. Rahman and J. C. Tully, *Journal of Chemical Physics*, 2002, **116**, 8750-8760.
38. S. Scheiner and E. A. Hillenbrand, *Journal of Physical Chemistry*, 1985, **89**, 3053-3060.
39. P. L. Geissler, C. Dellago, D. Chandler, J. Hutter and M. Parrinello, *Science*, 2001, **291**, 2121-2124.
40. D. Marx, M. E. Tuckerman, J. Hutter and M. Parrinello, *Nature*, 1999, **397**, 601-604.

41. F. A. Long and J. G. Pritchard, *Journal of the American Chemical Society*, 1956, **78**, 2663-2667.
42. J. G. Pritchard and F. A. Long, *Journal of the American Chemical Society*, 1956, **78**, 2667-2670.
43. J. F. Bunnett, *Journal of the American Chemical Society*, 1961, **93**, 4956-4967.
44. M. Tuckerman, K. Laasonen, M. Sprik and M. Parrinello, *Journal of Physical Chemistry*, 1995, **99**, 5749-5752.
45. G. Perdoncin and G. Scorrano, *Journal of the American Chemical Society*, 1977, **99**, 6983-6986.
46. P. R. Andrews, G. D. Smith and I. G. Young, *Biochemistry*, 1973, **12**, 3492-3498.
47. F. Claeysens, J. N. Harvey, F. R. Manby, R. A. Mata, A. J. Mulholland, K. E. Ranaghan, M. Schuetz, S. Thiel, W. Thiel and H.-J. Werner, *Angewandte Chemie-International Edition*, 2006, **45**, 6856-6859.
48. G. A. Olah, *Journal of the American Chemical Society*, 1972, **94**, 808-&.
49. N. C. Cole-Filipiak, A. E. O'Connor and M. J. Elrod, *Environmental Science & Technology*, 2010, **44**, 6718-6723.
50. W. Mabey and T. Mill, *Journal of Physical and Chemical Reference Data*, 1978, **7**, 383-415.
51. A. I. Darer, N. C. Cole-Filipiak, A. E. O'Connor and M. J. Elrod, *Environmental Science & Technology*, 2011, **45**, 1895-1902.
52. M. P. Tolocka, M. Jang, J. M. Ginter, F. J. Cox, R. M. Kamens and M. V. Johnston, *Environmental Science & Technology*, 2004, **38**, 1428-1434.
53. J. Dommen, A. Metzger, J. Duplissy, M. Kalberer, M. R. Alfarra, A. Gascho, E. Weingartner, A. S. H. Prevot, B. Verheggen and U. Baltensperger, *Geophysical Research Letters*, 2006, **33**.
54. M. Kalberer, D. Paulsen, M. Sax, M. Steinbacher, J. Dommen, A. S. H. Prevot, R. Fisseha, E. Weingartner, V. Frankevich, R. Zenobi and U. Baltensperger, *Science*, 2004, **303**, 1659-1662.